Local defect structure of $Sr_3Co_2O_x$ ($5.64 \leqslant x \leqslant 6.60$): Evolution of crystallographic and magnetic states

J. M. Hill,[1,*] B. Dabrowski,[2] J. F. Mitchell,[1] and J. D. Jorgensen[1]
[1]*Materials Science Division, Argonne National Laboratory, Argonne, Illinois 60439, USA*
[2]*Department of Physics, Northern Illinois University, DeKalb, Illinois 60115, USA*
(Received 31 July 2006; published 17 November 2006)

We have extended the structural and magnetic phase diagrams of the bilayer Ruddlesden-Popper phase $Sr_3Co_2O_x$ beyond previously reported limits of $x \approx 6.1$ to $x=6.60$. The room temperature crystal structure for the $x=6.60$ material is orthorhombic with oxygen vacancies located in the apical position that links the two nominally CoO_2 layers in the perovskite block. An antiferromagnetic ground state is converted to ferromagnetic by moderate magnetic fields and high-temperature magnetic susceptibility data indicate short-range ferromagnetic order. We have also studied the oxygen defect structure of $Sr_3Co_2O_x$ in the range $5.64 \leqslant x \leqslant 5.80$. Oxygen vacancies are present in both the in-plane sites, as well as the linking apical site. Critically, this linking site is displaced significantly along $\hat{z}$ from its ideal position, creating a particularly short Co-O bond. Using a combination of neutron powder diffraction (NPD) data and crystal-chemical considerations, we provide a model of the local Co ion environments. Additionally, low-temperature NPD and magnetization data show that the magnetic ground state of these oxygen-deficient materials is a complex antiferromagnet, with considerable sensitivity to precise oxygen content.

DOI: 10.1103/PhysRevB.74.174417 PACS number(s): 75.30.Cr, 61.12.Ld, 72.80.Ga

I. INTRODUCTION

Since the discovery of high-T_c superconductivity in a doped La-based $n=1$ Ruddlesden-Popper (R-P) phase copper oxide twenty years ago,[1,2] scientists have looked for similarly exciting physics in R-P phases containing other transition metals. So far, superconductivity has not been found, rather the doped R-P manganites exhibit colossal negative magnetoresistance.[3] An undoped Ag(II) analog has recently been shown to be a two-dimensional (2D) Heisenberg ferromagnet,[4] in contrast to the undoped copper oxides which have a Mott-insulating antiferromagnetic ground state.

Although perovskite and related cobalt oxides have been heavily studied over the past decade, due to the presence of novel charge, orbital and spin state phenomena, it is only recently that R-P Co phases have garnered interest. J. Matsuno *et al.* (Ref. 5) have found that epitaxial films of the $n=1$ R-P phase Sr_2CoO_4 are metallic ferromagnets with a relatively high $T_C \approx 250$ K. The observed saturation moment M_s was $1.8\mu_B$/Co. Subsequently, Wang and Takayama-Muromachi (Ref. 6) used high pressure, high temperature synthesis to prepare the compound in bulk polycrystalline form. Although these samples exhibited similar ferromagnetism, the resistivity ρ showed semiconducting behavior and $M_s \approx 1.0\mu_B$/Co. Recently, Lee and Pickett (Ref. 7) have investigated theoretically correlation effects in this material. Local density approximation (LDA) calculations show that the ground state of this material is a metallic ferromagnet with a moment near $2\mu_B$, in agreement with the behavior reported for the film. If, however, onsite Coulomb interactions are taken into account, there exists a half-metallic ferromagnetic state with $M_s=1\mu_B$/Co, consistent with the polycrystalline results. Oxygen defects may play a big role in determining whether or not correlations are important for this material.

From colossal magnetoresistance (CMR) manganite physics, it is well known that the $n=1$ and $n=2$ R-P phases have very different properties. The $n=2$ member of the Sr-Co-O R-P phase has been reported by Dann and Weller (Ref. 8) as an oxygen-deficient phase $Sr_3Co_2O_x$, $5.78 \leqslant x \leqslant 6.06$. They reported that samples with $x<6$ adopt orthorhombic structures with ordered oxygen vacancies along one axis in the CoO_2 plane. Samples with $x>6$ adopt the ideal R-P tetragonal structure. Recently, Viciu and coworkers (Ref. 9) observed complex magnetic behavior in similar compounds ($5.38 \leqslant x \leqslant 5.91$). Although they observed no ordering of oxygen vacancies in NPD data, ordering was observed in electron diffraction measurements. Samples with $x>6$ have been observed to react quickly with the air to form an oxyhydroxide $Sr_3Co_2O_5(OH)_2 \cdot yH_2O$.[10] Maignan and coworkers (Refs. 11 and 12) found cluster- and spin-glass-like properties in $x>6$ oxides and oxyhydroxides that contained partial substitution of Ti and Nb for Co.

To extend the materials chemistry and physics of the R-P series of cobaltites, we have synthesized the $n=2$ R-P phase $Sr_3Co_2O_x$, $5.64 \leqslant x \leqslant 6.60$, in bulk polycrystalline form. The strategy is to exploit the formation of oxygen vacancies to both tune the $Co^{2+}/Co^{3+}-Co^{3+}/Co^{4+}$ ratio and the coordination geometry (and potentially the spin-state) of the Co ion. Additionally, this compound allows us to study the properties of oxygen vacancy defect structures, which may not only be important in this series, but also play an important role in the properties of other cobaltites, such as $RBaCo_2O_{5+\delta}$.[13]

We find that the local oxygen defect structure across the series can be successfully modeled from average structural data (neutron powder diffraction) under the constraint of reasonable crystal-chemical considerations. The model is validated through bond-valence sum calculations and represents a new statistical, self-consistent approach to deconvoluting local structure from diffraction data. Using this approach we shed new light on the local crystallographic structures of both oxygen deficient ($x \approx 5.7$) and oxygen rich ($x=6.6$) samples. Like Viciu *et al.* (Ref. 9), we find that the $x<6$

samples are antiferromagnets with a complex temperature dependence and a weak ferromagnetic component. The newly synthesized $x=6.6$ sample, however, is found to be a low-temperature antiferromagnet that exhibits a field-induced transition to an extremely soft ferromagnet with an estimated saturation moment of $M_s=0.8(1)\mu_B/\mathrm{Co}$. This behavior is pre-saged by clear evidence of ferromagnetic short-range order observed in the temperature-dependent magnetization data. Extrapolation of the evolving magnetic properties indicates that the stoichiometric $x=7.0$ compound should be a long-range ordered ferromagnet, as reported for the fully oxidized $n=1$ phase.

II. EXPERIMENTAL DETAILS

Samples of $Sr_3Co_2O_x$ ($5.64 \leqslant x \leqslant 5.80$) were synthesized by calcining stoichiometric quantities of high purity $SrCO_3$ and Co_3O_4 (Alfa Aesar) in air at 1000 °C for 24 h. The resulting powder was subsequently heated in flowing ultra high purity (UHP) Ar at 1100 °C for several days with intermediate regrindings, then pelletized and sintered at 1100 °C. (The $x=5.64$ sample was made with Ar that was passed through a hot titanium charge.) A portion of this material was then annealed in UHP O_2 at 300 °C to produce compounds with $x \approx 6.5$. The oxygenated samples were carefully protected from the laboratory atmosphere at all times, to keep them from converting to $Sr_3Co_2O_5(OH)_2 \cdot yH_2O$.[9,10]

Samples were characterized by powder x-ray diffraction (XRD) on a PANalytical X'Pert Pro x-ray diffractometer with Co $K\alpha$ radiation. Lattice parameters were obtained using the software package Topas.[14] *In situ* oxygen annealing studies were carried out by loading approximately 0.5 g of $Sr_3Co_2O_{5.71}$ into the flat plate Al_2O_3 sample holder of an Anton Paar HTK 1200N high-temperature oven chamber affixed to the X'Pert Pro goniometer. The holder oscillated during data collection.

Oxygen contents were determined by reducing samples to their stable constituents SrO and Co in thermogravimetric analyzers (TGA) in a H_2/Ar atmosphere. The purpose was to obtain an accurate reference point for use in other TGA measurements where only changes in oxygen contents were measured and to compare to oxygen contents obtained from Rietveld refinements of neutron powder diffraction data. Empty crucible TGA runs were used for calibration and buoyancy corrections. The precision of the weight measurement was 2 μg. For measurements in the Perkin-Elmer TGA 7 equipped with a high-temperature furnace, approximately 50 mg of powder were placed in a Pt pan suspended from a Pt wire and heated to 900 °C at 1 °C/min in flowing 5.027% H_2/Ar. The estimated error on the oxygen content, based on weight loss during a 6.7 h hold at 900 °C, is ±0.01. For measurements in the Cahn TG171 system, 0.4–0.9 g of small chunks were placed in alumina crucibles suspended on Mo wires and heated to 1100 °C in flowing 50% H_2/Ar. No sublimation of Sr or Co was observed visually, however, small changes in the weight of samples held at 1100 °C for 2 h may indicate that such problems do exist at this temperature. These measurements imply that the error in the measured oxygen content is smaller than ±0.03. Oxygen annealing experiments were also performed in the Cahn TG171 using O_2 gas with a 1 °C/min sweep rate.

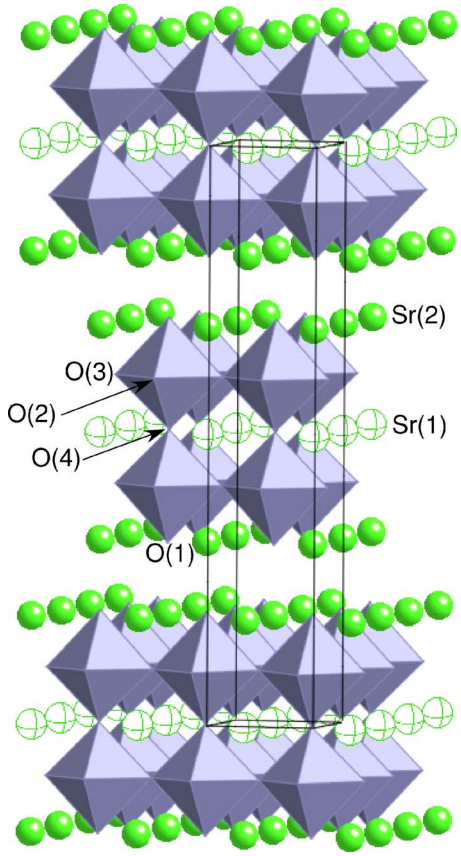

FIG. 1. (Color online) The ideal $n=2$ tetragonal Ruddlesden-Popper crystal structure [space group $I4/mmm$ (#139)] showing the bilayer structure of corner-shared CoO_6 octahedra.

Synchrotron x-ray diffraction (SXRD) data were collected at a wavelength of 0.619362 Å at the 1-ID beamline at the Advanced Photon Source at Argonne National Laboratory. Samples were sealed under Ar in 0.0340(5)″ O.D. polyimide capillary tubes and spun continuously during data collection. The data were analyzed using the software package CMPR.[15]

Neutron powder diffraction (NPD) studies were carried out at the Special Environment and General Purpose Powder Diffractometers (SEPD and GPPD, respectively) at the Intense Pulsed Neutron Source at Argonne National Laboratory.[16] Typical data collection times were 8–16 h for samples ranging in size from 2.5–10 g. Full-pattern Rietveld analysis of the time-of-flight diffraction patterns from detector banks located at 145 ° was accomplished using GSAS[17] and EXPGUI[18] software packages.

Magnetization M versus temperature T and applied magnetic field H data below 320 K were collected using a Quantum Design Physical Property Measurement System. No measurable contribution to the magnetization from ferromagnetic impurities was observed.

III. CRYSTAL STRUCTURE

A. $Sr_3Co_2O_x$, $x<6$

The ideal tetragonal $n=2$ R-P phase crystal structure [space group $I4/mmm$ (#139)] is shown in Fig. 1. It contains

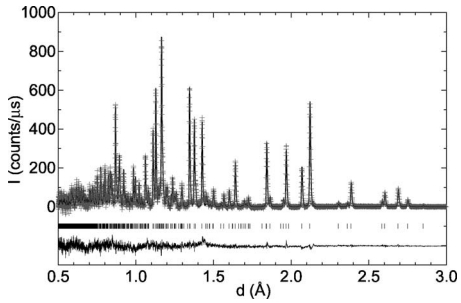

FIG. 2. Neutron powder diffraction data (+) collected on $Sr_3Co_2O_{5.71}$ sample B showing reflections (|) in the *Immm* space group (#71) for lattice parameters a=3.93347(6) Å, b =3.68182(6) Å, and c=20.6769(3) Å. The gray line through the data points is a Rietveld fit and the black line at the bottom of the figure is the difference curve [*I*(obs)-*I*(calc)].

corner-shared Co^{4+} octahedra that form bilayers of flat CoO_2 sheets. Powder diffraction data (representative NPD data are shown in Fig. 2) show that the compounds discussed in this paper have an orthorhombically distorted structure. The data are indexed in the *Immm* (#71) space group. Room temperature lattice parameters for the samples are shown in Table I. This result is consistent with an earlier report by Viciu and coworkers (Ref. 9) on similar oxygen content samples. They found that the O site which links the bilayers together [here called O(4), see Fig. 1] is displaced along $\hat{z}$ away from the ideal site (0,0,0). Additionally, their x=5.64 and 5.38 samples showed a small displacement of the other apical site [here called O(1)] along the $\hat{y}$ direction. The partially occupied O sites reported by Viciu *et al.* were the O(4) site and the in-plane *b*-axis O site [here called O(3)].

Results of Rietveld refinements performed on NPD data collected on our samples are shown in Table II, A–D. The crystallographic model presented here assumes disorder of the oxygen vacancies because there is no evidence for ordering seen in our NPD data. We find a large anisotropic thermal parameter ($U_{11} \approx 0$, $U_{22} \approx 0$, $U_{33} \approx 10$) when O(4) is placed at its ideal site of (0,0,0). Refinement of this model leads to the displacement of O(4) along $\hat{z}$ into the (0,0,z) position. However, we find no evidence for a displacement of O(1) along $\hat{y}$, even in our x=5.64 sample (sample D). Additionally, we find oxygen vacancies along *both* in-plane axes [O(2) and O(3)] and in the displaced O(4) site. The thermal parameters of the in-plane sites remained highly anisotropic, indicating significant in-plane displacements along directions with a large vacancy concentration, but the inability to fit these displacements by placing some of these atoms in displaced sites suggests that the displacement directions and magnitudes are randomized by local interactions associated with the large defect concentration. The isotropic thermal parameter of the displaced O(4) site could not be refined simultaneously with the site occupancy and so it was fixed at 1.

Considering the $Sr_3Co_2O_7$ end member as a starting point, the local effect of an oxygen vacancy in the CoO_2 plane is a decrease of the Co oxidation state (from 4+ to 3+), due to the formation of Co square pyramids rather than octahedra. (Square-pyramidal coordination is typical for Co^{2+}/Co^{3+} oxides, cf. $RBaCo_2O_5$.[13]) However, the bond valence sum (BVS) of a square pyramid in $Sr_3Co_2O_x$, $x<6$ is 2.58, when $R_{Co^{3+}}$=1.70 Å[19] is used *and* the O(4) atom is left in its ideal position (0,0,0). In other words, the Co^{3+} is underbonded. To counter this effect, the structure responds by pulling an apical oxygen in closer to the Co. This is manifest in the observed displacement of O(4) along $\hat{z}$ by $\pm z$. The consequence is that two Co-O(4) bonds are created: a short one ($\approx$1.8 Å), which has the effect of increasing the BVS of the Co square pyramid to a more reasonable 2.95, and a long one ($\approx$2.3 Å), which can be considered nonbonding (see Table III). In this way the square pyramidally coordinated Co is able to maintain its 3+ character.

Initially, we tried to refine the NPD data using a structural model that contained no O(2) vacancies. However, when the occupancy of the O(2) site was allowed to vary, the vacancy concentration on the O(2) site was found to refine to $\approx$7%, with a statistically better fit to the NPD data than leaving it fixed at 1.0. This finding is relevant to the analysis of the local coordination polyhedra found in the compound. To explore the types and frequencies of the various Co coordination units present, we constructed several supercell models (containing 10 unit cells) decorated statistically with O vacancies ($x \approx 5.7$). We found that $\approx$7% of the Co sites were octahedra. In the context of this statistical model, the NPD refinement of $\approx$7% O(2) vacancies implies that no Co^{4+} octahedra are found in the structure, a result that is consistent with the average low Co oxidation state in the compound.

Diffraction models per force allow direct access only to average, statistical information in disordered compounds, such as the present system. It is clear, however, that the local structure is critical for understanding the Co oxidation state,

TABLE I. Room temperature lattice parameters and oxygen content for $Sr_3Co_2O_x$ determined from Rietveld refinements of neutron powder diffraction. The space group is orthorhombic *Immm* (#71).

Sample Code	x^a	x^b	a (Å)	b (Å)	c (Å)	V (Å^3)
A	5.80(5)	5.79(3)	3.92741(4)	3.68277(4)	20.6587(2)	298.801(4)
B	5.71(5)	5.83(3)	3.93347(6)	3.68182(6)	20.6769(3)	299.449(6)
C	5.73(5)	5.71(1)	3.93395(8)	3.67982(7)	20.6555(4)	299.014(7)
D	5.64(5)	—	3.93974(8)	3.67437(7)	20.6627(4)	299.115(7)
E	6.60(1)	6.62(3)	3.83846(5)	3.82703(5)	20.0698(2)	294.824(4)

[a]Determined from neutron powder diffraction.
[b]Determined from thermogravimetric analysis.

TABLE II. The atomic positions, occupancies, and thermal parameters determined from Rietveld refinements of room temperature neutron powder diffraction data for $Sr_3Co_2O_x$. The space group is orthorhombic *Immm* (#71).

Sample	Atom	Site	x	y	z	Occ.	U_{11}; U_{22}; U_{33}; [U_{iso}] ($\times 100$) Å^2
	Sr(1)	2*c*	1/2	1/2	0	1	1.9(1); 2.7(1); 1.0(1)
A	Sr(2)	4*i*	0	0	0.31429(7)	1	[1.40(5)]
R_{wp}=5.64%	Co	4*i*	0	0	0.1005(1)	1	[0.45(7)]
R_p=4.15%	O(1)	4*i*	0	0	0.19464(8)	1	[1.01(5)]
χ^2=3.254	O(2)	4*j*	1/2	0	0.0942(1)	0.91(1)	3.5(2); 2.3(2); 1.5(2)
	O(3)	4*j*	0	1/2	0.0837(2)	0.66(1)	4.5(3); 0.8(2); 5.4(3)
	O(4)	4*i*	0	0	0.0123(3)	0.328(5)	1
	Sr(1)	2*c*	1/2	1/2	0	1	2.1(2); 2.4(2); 1.0(1)
B	Sr(2)	4*i*	0	0	0.31415(9)	1	[1.49(6)]
R_{wp}=5.52%	Co	4*i*	0	0	0.1000(2)	1	[1.0(1)]
R_p=4.03%	O(1)	4*i*	0	0	0.1948(1)	1	[1.31(6)]
χ^2=1.742	O(2)	4*j*	1/2	0	0.0943(2)	0.93(1)	4.3(2); 2.3(2); 1.9(2)
	O(3)	4*j*	0	1/2	0.0826(2)	0.63(1)	4.2(3); 1.1(2); 4.6(3)
	O(4)	4*i*	0	0	0.0124(3)	0.293(5)	1
	Sr(1)	2*c*	1/2	1/2	0	1	1.8(2); 3.1(2); 1.0(2)
C	Sr(2)	4*i*	0	0	0.3143(1)	1	[1.63(7)]
R_{wp}=4.20%	Co	4*i*	0	0	0.1004(3)	1	[0.54(9)]
R_p=3.08%	O(1)	4*i*	0	0	0.1947(1)	1	[1.33(6)]
χ^2=1.733	O(2)	4*j*	1/2	0	0.0934(2)	0.97(1)	4.6(3); 2.8(2); 2.5(2)
	O(3)	4*j*	0	1/2	0.0834(3)	0.60(1)	3.3(4); 0.0(1); 6.3(4)
	O(4)	4*i*	0	0	0.0130(4)	0.296(6)	1
	Sr(1)	2*c*	1/2	1/2	0	1	2.7(2); 2.6(2); 1.0(2)
D	Sr(2)	4*i*	0	0	0.3142(1)	1	[1.77(7)]
R_{wp}=5.80%	Co	4*i*	0	0	0.1000(3)	1	[1.2(1)]
R_p=4.25%	O(1)	4*i*	0	0	0.1946(1)	1	[1.42(7)]
χ^2=1.786	O(2)	4*j*	1/2	0	0.0936(2)	0.95(1)	4.1(2); 2.8(2); 2.5(2)
	O(3)	4*j*	0	1/2	0.0819(3)	0.59(1)	4.2(4); 0.4(3); 5.2(4)
	O(4)	4*i*	0	0	0.0130(4)	0.279(6)	1
	Sr(1)	2*c*	1/2	1/2	0	1	[1.18(4)]
E	Sr(2)	4*i*	0	0	0.31836(5)	1	[0.93(3)]
R_{wp}=4.52%	Co	4*i*	0	0	0.0989(1)	1	[0.63(5)]
R_p=3.33%	O(1)	4*i*	0	0	0.19446(8)	1	[1.19(3)]
χ^2=2.839	O(2)	4*j*	1/2	0	0.0912(3)	1	[0.99(8)]
	O(3)	4*j*	0	1/2	0.0908(3)	1	0.8(1); 0.9(1); 2.6(1)
	O(4)	2*a*	0	0	0	0.604(9)	0.9(1)

potential spin states, magnetism, etc. Here we propose to explore the local coordination geometry using as input the refined oxygen concentrations and a few reasonable assumptions about the chemistry of Co^{2+} and Co^{3+}. To generate a model of the local structure of $Sr_3Co_2O_x$, $x<6$, we apply a set of "rules" that require the structural model to be self-consistent with the NPD refinement and accepted crystal-chemistry considerations. The model is validated by computing the average bond-valence sum (BVS) and comparing it to the oxidation state extracted from the NPD refinement. Similar appeals to BVS calculations are routinely used to assign crystallographic site occupancies, test the reasonableness of structural models, etc. To our knowledge, this is the first time an oxide defect structure has been decomposed into constituent coordination polyhedra and analyzed via BVS constraints. We believe such an approach may be useful in other cases where average and local structures are clearly different.

For the present case, the rules and their rationale are

(1) Short Co-O(4) bonds are created by in-plane oxygen vacancies to prevent Co underbonding.

(2) There are no short-bond tetrahedra, guaranteeing only Co^{2+} with tetrahedral coordination.

(3) To avoid an unphysical square planar geometry for Co, no Co site can have two in-plane oxygen vacancies.

(4) An O(2) vacancy is always found in a short-bond square pyramid.

TABLE III. The Co-O bond distances for $Sr_3Co_2O_x$ at room temperature.

Bonds	Bond distances (Å)				
	A	B	C	D	E
Co-O(1)	1.945(4)	1.963(5)	1.946(5)	1.955(6)	1.917(3)
Co-O(2)×2	1.9680[a]	1.9703(4)[a]	1.9723(6)[a]	1.9743(5)[a]	1.9256(4)
Co-O(3)×2	1.8740(8)[a]	1.876(1)[a]	1.873(1)[a]	1.875(1)[a]	1.9204(5)
Co-O(4)[a]	1.822(6), 2.331(7)[b]	1.812(8), 2.323(9)[b]	1.806(9), 2.34(1)[b]	1.797(9), 2.34(1)[b]	1.986(3)

[a]Partially occupied.

[b]This site links two Co atoms in the bilayer along the $\hat{z}$ direction. When this site is occupied (approximately 60% of the time), the occupying O atom is displaced from the ideal site (0,0,0) along $\hat{z}$ by $\pm z$, creating a short, "bonding" and long, "nonbonding" bond.

The above rules generate a self-consistent crystal structure made up of three types of Co polyhedra: short-bond square pyramids, square pyramids, and tetrahedra. The possible configurations are shown in Fig. 3. Co oxidation states of 3+, 2+/3+, and 2+, respectively, can be associated with these coordinations using BVS calculations. From these configurations and the NPD refinement, the average BVS of the structure can be calculated to test for self-consistency. There does remain one ambiguity when applying these rules: It is not possible to determine the percentage of O(2) vacancies that yield short-bond square pyramids versus tetrahedra from the site occupancies alone. We have chosen to place all the O(2) vacancies in short-bond square pyramids, because that produces a square pyramidal BVS closest to the ideal value of 3. The tetrahedra in this case have one O(3) site missing and have a BVS of 2, consistent with the expected oxidation state of Co in a tetrahedron. The other limiting case, placing all O(2) vacancies in tetrahedra, is not desirable because this drives the BVS of the tetrahedra (short-bond square pyramids) higher (lower) than the ideal value of 2 (3).

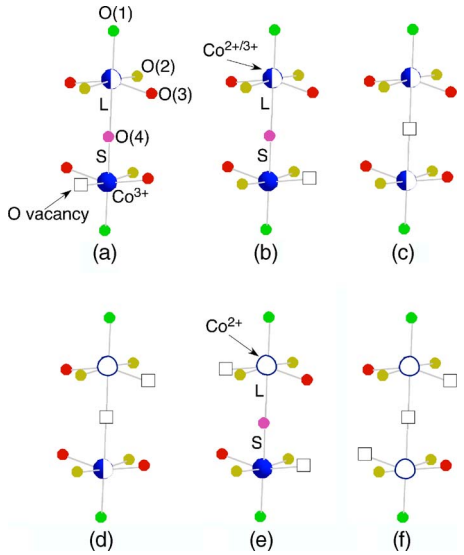

FIG. 3. (Color online) The Co polyhedra found in $Sr_3Co_2O_x$, $x < 6$. Large open circles represent Co^{2+}; large filled circles represent Co^{3+}, and open squares show oxygen vacancies. S and L refer to a short Co-O(4) bond and a long Co-O(4) bond, respectively (see Table III). (a) and (b) Short-bond Co^{3+} square pyramids containing an O(2) or O(3) vacancy linked to long-bond $Co^{2+/3+}$ square pyramids. (c) Two $Co^{2+/3+}$ square pyramids created by a vacancy on the O(4) site. (d) A Co^{2+} tetrahedra linked to a $Co^{2+/3+}$ square pyramid. (e) A Co^{2+} tetrahedra linked to a Co^{3+} square pyramid. (f) Two Co^{2+} tetrahedra linked by an O(4) vacancy.

Validation of the model via BVS calculation is most easily seen through example. Figure 4 shows how the average BVS for the structure is calculated using the refinement results from sample B. The site occupancy of the split O(4) site for this sample is 0.293. A short-bond square pyramid is associated with this site being occupied; therefore, the percentage of short bonds in the structure is simply twice the occupancy of the O(4) site, or 58.6%. (The factor of two is introduced because the *ab* plane is a mirror plane in the *Immm* space group.) Applying rule 4, the percentage of these short-bond square pyramids that contain an O(2) vacancy is simply the total percentage of O(2) vacancies, which for sample B is 7%. The rest of the short-bond square pyramids 51.6% contain an O(3) vacancy. The percentage of O(3) va-

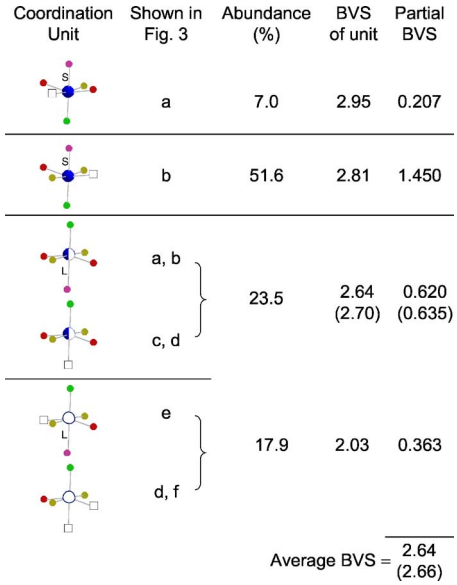

FIG. 4. (Color online) A bond valence sum (BVS) calculation illustrated for sample B. Partial BVSs are calculated by multiplying the unit BVSs by their percentage occurrence in the structure. The average BVS is the sum of the partial BVSs. The BVS of the Co^{2+} tetrahedral (Co^{3+} square pyramidal) units is calculated using $R_{Co^{2+}}$ ($R_{Co^{3+}}$) (Ref. 19). The mixed valent unit BVS is calculated using $R_{Co^{2+}}$ ($R_{Co^{3+}}$).

TABLE IV. A comparison of the Co oxidation state determined from neutron powder diffraction (NPD) and calculated bond valence sums (BVS).

Sample	NPD	BVS[a]
A	2.80(5)	2.70 (2.71)
B	2.71(5)	2.64 (2.66)
C	2.73(5)	2.67 (2.69)
D	2.64(5)	2.70 (2.72)

[a]The values in parentheses are obtained if $R_{Co^{3+}}$ is used for the mixed-valent Co square pyramids.

cancies associated with the short-bond square pyramids is 51.6% × 37% (the total amount of vacancy on the O(3) site) or 19.1%. The remaining O(3) vacancies (37%−19.1% =17.9%) create tetrahedra. This analysis accounts for 76.5% of the Co atoms (58.6%+17.9%=76.5%). The Co atoms still unaccounted for form mixed valent 2+/3+ square pyramids. As shown in Fig. 3, they are connected to either long Co-O(4) bonds or O(4) vacancies.

The BVS can be calculated for each polyhedral type discussed above, using the usual formula with $R_{Co^{3+}}=1.70$ for the short-bond square pyramids and $R_{Co^{2+}}=1.692$ for the tetrahedra.[19–22] The BVS for the mixed valent units was calculated using both $R_{Co^{2+}}$ ($R_{Co^{3+}}$). As outlined in Fig. 4, the contribution to the BVS for each polyhedral type is calculated by multiplying its individual BVS by its frequency in the structure. For example, the short-bond square pyramids that contain on O(2) vacancy have a BVS=2.95. Therefore, their contribution is 2.95×7% or 0.207. The average BVS for the structure is simply the sum of all the partial BVSs.

The result of the foregoing analysis for all the $Sr_3Co_2O_x$, $x<6$ samples is reported in Table IV along with a comparison to the oxygen contents determined from NPD refinements. It should be noted that this local structure model is purely statistical and does not account for correlations among types of polyhedra enforced by the lattice. Likewise, the BVS approach itself is only semiquantitative. The agreement between BVS values derived from the model and the oxidation state calculated from the oxygen stoichiometry is excellent given such limitations, and gives us confidence that the model is a sensible representation of the local defect structure.

B. $Sr_3Co_2O_x$, $x>6$

$Sr_3Co_2O_x$, $x\approx6.5$ can only be made by annealing the $Sr_3Co_2O_x$, $x<6$ material in O_2 gas at low temperatures. XRD data from an *in situ* oxidation experiment are shown in Fig. 5(a). The first-formed product is tetragonal and indexes in the $I4/mmm$ (#139) space group with lattice parameters $a=3.86099(5)$ Å and $c=20.1787(4)$ Å at $T=315$ °C. Upon cooling the sample below 150 °C, several reflections gradually began to broaden, particularly those with $h\neq k$, see Fig. 5(b). However, it was not possible to define an exact phase transition temperature, given the limited resolution of the lab x-ray source. Different cooling rates and hold times did not change the results. Importantly, an oxidation experiment performed in a TGA, shown in Fig. 6, shows that the oxygen content of the sample remains constant below $T\approx150$ °C. Therefore, the broadening observed in the *in situ* XRD is not due to changes in oxygen content.

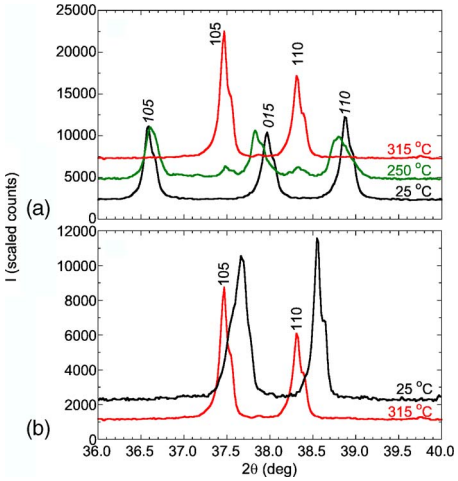

FIG. 5. (Color online) (a) Co $K\alpha$ x-ray diffraction patterns of $Sr_3Co_2O_x$, $x<6$ collected *in situ* during heating in flowing UHP O_2. The intensities of the $T=250$ °C and 315 °C patterns were shifted up by 2500 and 5000 counts, respectively, for clarity. (b) Co $K\alpha$ x-ray diffraction patterns of $Sr_3Co_2O_x$, $x>6$, collected *in situ* during cooling in flowing UHP O_2. The intensity of the $T=315$ °C pattern was multiplied by 0.5 for clarity. The italicized Miller indices for space group *Immm* mark the starting material, whereas the nonitalicized Miller indices are for the high-temperature tetragonal $I4/mmm$ phase.

The *in situ* oxygen-annealed sample described above could not be preserved, due to reaction with air; therefore, oxidized samples for further measurements were prepared in a separate furnace using similar conditions. A room temperature SXRD measurement, shown in Fig. 7, clearly shows that the room temperature structure of the $x>6$ compound is orthorhombic. Least-squares fits to the individual peaks using a pseudovoigt function, shown in the figure as solid gray lines, reveal that the full width at half maximum of reflections of the type *hkl* broaden while the *hhl* remain sharp. This is consistent with the appearance of an orthorhombic strain and eventually a phase transition to *Immm*. The lattice parameters for the SXRD sample are $a=3.84234(2)$ Å, $b=3.82361(2)$ Å, and $c=20.0919(1)$ Å. There is a large con-

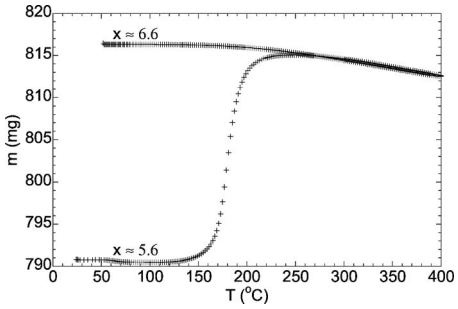

FIG. 6. An oxidation experiment on a sample of $Sr_3Co_2O_x$ performed in a thermogravimetric analyzer in pure O_2.

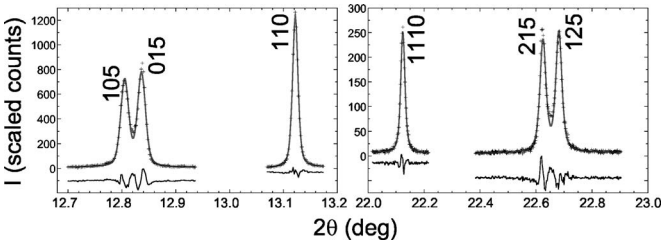

FIG. 7. Room temperature synchrotron x-ray diffraction data (+) of $Sr_3Co_2O_x$, $x>6$ collected at $\lambda=0.619362$ Å. The thick solid gray lines are least-square fits to the individual peaks using a pseudovoigt function. The difference curves are shown as thin solid black lines. The peaks are indexed in the orthorhombic space group *Immm* (#71).

traction of the c axis in this oxidized material, consistent with the formation of the small ion Co^{4+}.

Room temperature NPD data for another oxidized compound, sample E, are shown in Fig. 8 with refined crystallographic parameters tabulated in Tables I and II. The oxygen vacancies in this compound lie only in the O(4) site. The occupancies of the O(2) and O(3) sites refined to >1 and were, therefore, fixed at one in the final refinement. Although the in-plane O sites are filled, the CoO_2 sheets are not flat, due to an asymmetric umbrella motion of the O(2) and O(3) atoms, leading to the observed orthorhombic structure. The isotropic thermal parameters reflect typical values observed in oxides, with the exception of O(3). Its thermal parameter is oriented mostly along $\hat{z}$. The small isotropic thermal parameter for the O(4) site indicates that these oxygen atoms are no longer displaced along $\hat{z}$, as expected for a material containing no in-plane oxygen vacancies. As discussed above in Rule (1), it is the in-plane oxygen vacancies which drive the displacement of the oxygen atoms in this site to compensate for Co^{3+} underbonding. If there are no vacancies present, then there is no need to displace the O(4) atoms.

The Co oxidation state determined from NPD is 6.60(1), which agrees well with the valued obtained from mass gain measurements, 6.62(3). In this case, only two kinds of polyhedra are found: square pyramids and octahedra. A straightforward appeal to crystal chemistry assigns the former to Co^{3+} and the latter to Co^{4+}. The BVS for Co^{4+} cannot be

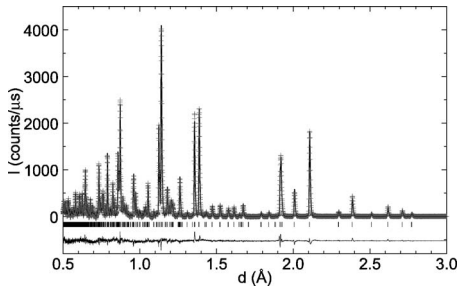

FIG. 8. Neutron powder diffraction data (+) collected on $Sr_3Co_2O_{6.60}$ sample E showing reflections (|) in the *Immm* space group (#71) for lattice parameters a=3.83846(5) Å, b =3.82703(5) Å, and c=20.0698(2) Å. The gray line through the data points is a Rietveld fit and the black line at the bottom of the figure is the difference curve [I(obs)-I(calc)].

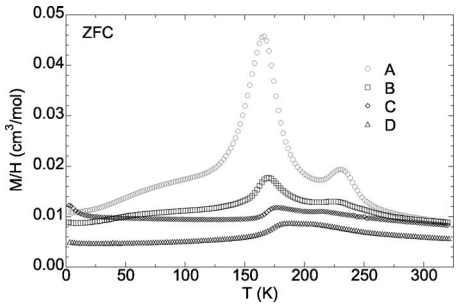

FIG. 9. Magnetization divided by magnetic field vs temperature data for $Sr_3Co_2O_x$ samples A (○), B (□), C (◇), and D (△). For clarity, the D data were shifted down by 0.003 cm^3/mol.

formally calculated since $R_{Co^{4+}}$ is not tabulated; however, the value obtained using $R_{Co^{3+}}$ is 3.21, indicating that the oxidation state at this site exceeds 3+. The percentage of Co^{4+} octahedra is equal to the occupancy of the O(4) site, 60.4%. The remaining 39.6% of the Co atoms form square pyramids (BVS=2.75).

IV. MAGNETIZATION MEASUREMENTS

A. $Sr_3Co_2O_x$, $x<6$

M/H data plotted as a function of T for the $Sr_3Co_2O_x$, $x<6$ samples are shown in Fig. 9. The magnetic properties vary dramatically with small changes in oxygen content. Sample D [$x=5.64(5)$] has only one transition (at $T \approx 180$ K) and a broad feature (at $T \approx 215$ K), both of which sharpen as oxygen is added. Moreover, these two features have a weak temperature dependence as well. The 180 K (215 K) feature decreases (increases) in temperature as oxygen is added. This supports the idea that the two-peak structure is intrinsic as opposed to it arising from the appearance of two fixed x line compounds (i.e. a miscibility gap).

Consistent with previous results by Viciu *et al.* (Ref. 9), $M(H)$ curves (not shown) reveal the onset of a small irreversibility below the higher-T peak that persists down to 2 K (the lowest measurement temperature), indicating a ferromagnetic contribution to the magnetization. However, NPD data collected at 20 K show several antiferromagnetic ordering reflections (marked by arrows in Fig. 10) confirming the

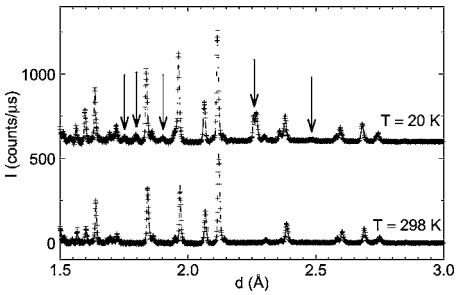

FIG. 10. Neutron powder diffraction data (+) collected on $Sr_3Co_2O_{5.73}$ sample C at 20 K and 298 K. The arrows highlight antiferromagnetic reflections. For clarity, the 20 K data were shifted up by 1200 counts/μs.

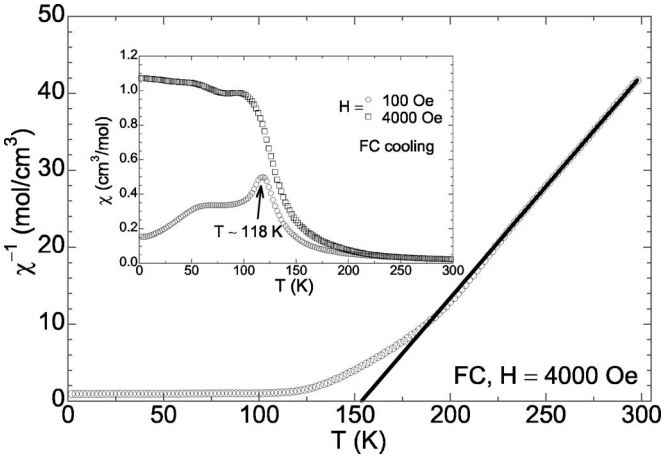

FIG. 11. Inverse magnetic susceptibility χ^{-1} vs temperature T field-cooled (FC) data (○) taken on cooling for $Sr_3Co_2O_{6.60}$ sample E. The solid line is a fit to the data from 234–298 K by a Curie-Weiss function with C=3.459(5) cm^3 K/mol and θ=153.6(6) K. Inset: $\chi(T)$ FC data taken in a magnetic field H=100 Oe (○) and 4000 Oe (□) for $Sr_3Co_2O_x$ sample E.

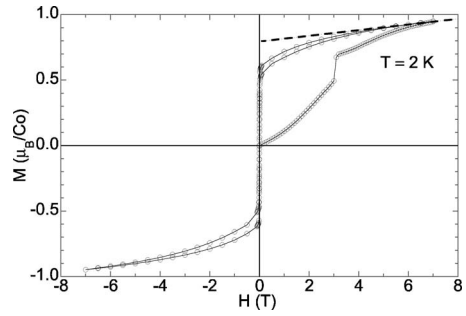

FIG. 12. Magnetization vs magnetic field data (○) for $Sr_3Co_2O_{6.60}$ sample E. The thin lines are guides to the eye. The dashed line is a linear fit from 6–7 T extrapolated to yield M_s =0.8(1)μ_B/Co.

antiferromagnetic ground state. Determination of the magnetic structure was handicapped by low resolution of the high d-spacing data (not shown in Fig. 10). Our preliminary results suggest that there may be multiple wave vectors and/or that the wave vector(s) may be incommensurate. Higher resolution experiments are necessary and in progress.

Although no evidence for oxygen ordering is seen in the XRD and NPD data for these materials, Viciu and coworkers (Ref. 9) have observed evidence for such behavior in electron diffraction studies and Dann *et al.* (Ref. 8) observed an oxygen superstructure in their NPD data. This suggests that small changes in oxygen content give rise to subtle changes in oxygen (vacancy) ordering which may contribute to the extreme sensitivity toward oxygen exhibited by the magnetic properties.

B. $Sr_3Co_2O_x$, $x>6$

Magnetic susceptibility $\chi(T)$ data for sample E are shown in the inset of Fig. 11. There are two transitions visible in the low-field (H=100 Oe) measurement: a sharp peak at $T\approx$118 K and a broad hump around $T\approx$60 K. The transition at 118 K is of antiferromagnetic character, as shown below by $M(H)$ measurements. Nonetheless, data measured in a 4 kOe applied field show substantially enhanced magnetization and a shift of the curve to higher temperature. Both effects indicate the presence of short-range ferromagnetic (FM) interactions. The inverse magnetic susceptibility $\chi^{-1}(T)$ data were fit to a Curie-Weiss function, yielding C =3.459(5) cm^3 K/mol and θ=153.6(6) K. The sign of the Weiss constant indicates that the high-temperature exchange is ferromagnetic, in agreement with the presence of FM short-range order noted above. The effective moment is 5.259(1)μ_B/f.u. consistent with both Co^{3+} and Co^{4+} adopting intermediate-spin (IS) configurations or with Co^{3+} in a high-spin (HS) state and Co^{4+} in a low-spin (LS) state. It is difficult to uniquely assign spin states based solely on the effective moment. However, assigning Co^{3+} to the square pyramidal sites of this oxygen-deficient structure implies a nonzero spin-state assignment at this site. In the case of $RBaCo_2O_5$, Co^{3+} in the pyramidal site adopts a HS state.[23–25] The pyramidal sites of $RBaCo_2O_{5.5}$ are considered IS by numerous authors. In the present case, neither the IS nor HS state is implausible due to the inductive effect of neighboring Co^{4+} ions, which will tend to reduce even further the crystal field at the five-coordinate Co^{3+} site. Nonetheless, even with the assumption of either HS Co^{3+} and LS Co^{4+} or IS Co^{3+} and Co^{4+}, the effective moment is somewhat less than that derived from the Curie-Weiss fit. It is possible that the discrepancy can be attributed to spin-orbit coupling enhancing the Landè factor ($g\approx$2.1) for both Co ions. Ultimately, a definitive assignment of spin states will require more direct probes, such as x-ray photoemission spectroscopy.

Low-temperature hysteresis loops confirm that the ground state is an antiferromagnet. Figure 12 shows a sharp step appearing at approximately 3 T in the 2 K virgin $M(H)$ data. The resulting ferromagnet is extremely soft, as evidenced by the lack of coercivity. Sharp steps such as these have been seen in manganites and attributed either to martensitic transformations or run-away heating. In these cases, the ZFC state is a mixture on the μm scale of an antiferromagnetic charge-ordered insulator and a ferromagnetic metal. The linear low-field magnetic susceptibility seen in Fig. 12 argues against such a scenario in the present case. That the threshold field ($H\approx$3 T) is reproducible on thermal cycling suggests that a fixed defect landscape, perhaps the oxygen defect structure, is the cause of this sharp transition rather than a phase competition as found in the manganites.

The magnetization is clearly not saturated by H=7 T, but the saturated portion can be estimated by extrapolating the high field data (6–7 T) to H=0, yielding a value for M_s =0.8(1)μ_B/Co. Such an estimate indicates that not all of the spins are fully polarized; if they were, a value slightly in excess of 1μ_B/Co would be expected for this mixed-valent compound. Alternatively, it is possible that the Co ions have undergone a transition to a lower spin state, though this seems unlikely, as the limiting case of the x=7.0 compound would yield M_s=1μ_B/Co for the case of LS Co^{4+}.

V. SUMMARY

We have synthesized $n=2$ R-P phases $Sr_3Co_2O_x$, $5.64 \leqslant x \leqslant 6.60$. These materials adopt an orthorhombically distorted *Immm* crystal structure at room temperature. For oxygen contents of $x<6$, oxygen vacancies are found in both in-plane sites, as well as the apical linking site. Additionally, the linking site is displaced along $\hat{z}$, creating a short Co-O(4) bond. The consequences of such a bond are developed in a self-consistent model of the local structure using a combination of the NPD data, crystal-chemistry, and BVSs. The resulting picture shows that Co is coordinated only by 3+ short-bond square pyramids, mixed valent 2+/3+ square pyramids and 2+ tetrahedra.

The magnetic properties of these materials are complex. The magnitude of the two peaks observed in the $M/H(T)$ data is extremely sensitive to oxygen content. The weak temperature dependence of this two-peak structure suggests that this feature is intrinsic and not a signature of a miscibility gap. Small hysteresis loops inside an overall antiferromagnetic $M(H)$ curve develop below the highest-T peak and remain to low temperature, indicating a weak ferromagnetic component. However, low T NPD data show that the ground state is indeed antiferromagnetic. One can speculate that some sort of canted state may exist at low T.

The as-formed $x>6$ material has a tetragonal high-temperature structure, whereas the room temperature structure is orthorhombic. Oxygen vacancies were found only in the linking O(4) site, which is located in its ideal position. The extended crystal structure is a simple mixture of Co^{3+} square pyramids and Co^{4+} octahedra.

Magnetically, this oxygen rich phase is an antiferromagnet with a pronounced degree of short-range ferromagnetic order. The ZFC low T $M(H)$ curve shows a reproducible metamagnetic transition at $H \approx 3$ T to a soft ferromagnet that does not saturate for $H \leqslant 7$ T. The extrapolated saturation moment of $M_s = 0.8(1)\mu_B/\mathrm{Co}$ nonetheless indicates that this is a substantially polarized state.

The evolution of magnetic behavior with decreasing oxygen defect concentration follows from weak ferromagnet through an antiferromagnet with considerable ferromagnetic short-range-order and a metamagnetic state. Extrapolation of these evolving properties indicates that the stoichiometric endmember compound should be a long-range ordered ferromagnet, as reported for the fully oxidized $n=1$ phase.

ACKNOWLEDGMENTS

We thank P. L. Lee and J. S. Fieramosca, A. Huq, and E. Maxey for assistance with the SXRD and NPD measurements, respectively. The work at Argonne National Laboratory was supported by the U.S. DOE Office of Science, Basic Energy Sciences, under Contract No. W-31-109-ENG-38. The work at Northern Illinois University was supported by the National Science Foundation under Contract No. NSF-DMR-0302617.

*Electronic address: jmhill@anl.gov

[1] J. G. Bednorz and K. A. Mueller, Z. Phys. B: Condens. Matter **64**, 189 (1986).
[2] R. J. Cava, R. B. van Dover, B. Batlogg, and E. A. Rietman, Phys. Rev. Lett. **58**, 408 (1987).
[3] Y. Moritomo, A. Asamitsu, H. Kuwahara, and Y. Tokura, Nature (London) **380**, 141 (1996).
[4] S. E. McLain, M. R. Dolgos, D. A. Tennant, J. F. C. Turner, T. Barnes, T. Proffen, B. C. Sales, and R. I. Bewley, Nat. Mater. **5**, 561 (2006).
[5] J. Matsuno, Y. Okimoto, Z. Fang, X. Z. Yu, Y. Matsui, N. Nagaosa, M. Kawasaki, and Y. Tokura, Phys. Rev. Lett. **93**, 167202 (2004).
[6] X. L. Wang and E. Takayama-Muromachi, Phys. Rev. B **72**, 064401 (2005).
[7] K.-W. Lee and W. E. Pickett, Phys. Rev. B **73**, 174428 (2006).
[8] S. E. Dann and M. T. Weller, J. Solid State Chem. **115**, 499 (1995).
[9] L. Viciu, H. W. Zandbergen, Q. Xu, Q. Huang, M. Lee, and R. J. Cava, J. Solid State Chem. **179**, 500 (2006).
[10] D. Pelloquin, N. Barrier, A. Maignan, and V. Caignaert, Solid State Sci. **7**, 853 (2005).
[11] T. Motohashi, B. Raveau, V. Caignaert, V. Pralong, M. Hervieu, D. Pelloquin, and A. Maignan, Chem. Mater. **17**, 6256 (2005).
[12] D. Pelloquin, N. Barrier, D. Flahaut, V. Caignaert, and A. Maignan, Chem. Mater. **17**, 773 (2005).
[13] D. D. Khalyavin, Phys. Rev. B **72**, 134408 (2005), and cited references.
[14] URL http://www.bruker-axs.de
[15] B. H. Toby, J. Appl. Crystallogr. **38**, 1040 (2005).
[16] J. D. Jorgensen, J. Faber, Jr., J. M. Carpenter, R. K. Crawford, J. R. Haumann, R. L. Hitterman, R. Kleb, G. E. Ostrowski, F. J. Rotella, and T. G. Worlton, J. Appl. Crystallogr. **22**, 321 (1989).
[17] A. C. Larson and R. B. von Dreele, LAUR 86–748, Los Alamos National Laboratory (2000).
[18] B. H. Toby, J. Appl. Crystallogr. **34**, 210 (2001).
[19] N. E. Brese and M. O'Keeffe, Acta Crystallogr., Sect. B: Struct. Sci. **B47**, 192 (1991).
[20] I. D. Brown and D. Altermatt, Acta Crystallogr., Sect. B: Struct. Sci. **B41**, 244 (1985).
[21] M. O'Keeffe and N. E. Brese, J. Am. Chem. Soc. **113**, 3226 (1991).
[22] M. O'Keeffe and N. E. Brese, Acta Crystallogr., Sect. B: Struct. Sci. **B48**, 152 (1992).
[23] E. Suard, F. Fauth, V. Caignaert, I. Mirebeau, and G. Baldinozzi, Phys. Rev. B **61**, R11871 (2000).
[24] J. C. Burley, J. F. Mitchell, S. Short, D. Miller, and Y. Tang, J. Solid State Chem. **170**, 339 (2003).
[25] M. Soda, Y. Yasui, M. Ito, S. Iikubo, M. Sato, and K. Kakurai, J. Phys. Soc. Jpn. **73**, 464 (2004).